HSP90 inhibitor gedunin impairs glioblastoma proliferation and invasiveness

Thadeu Estevam Moreira Maramaldo Costa[a,b], Tatiana Almeida Pádua[b], Jonathas Xavier Pereira[c], Vinicius Gonçalves Rodrigues[c], Leonardo Noboru Seito[b], Erika Marques da Cunha[b], Claudio C. Filgueiras[d], Yael Abreu-Villaça[d], Alex C. Manhães[d], Clarissa Menezes Maya-Monteiro[e,f], Maria das Graças Henriques[b,g], Thomas Eichenberg Krahe[d,h], Carmen Penido[a,b,*]

[a] Centro de Desenvolvimento Tecnológico em Saúde, Instituto Nacional de Ciência e Tecnologia de Inovação em Doenças Negligenciadas (INCT-IDN), Fundação Oswaldo Cruz, Rio de Janeiro, Brazil.

[b] Laboratório de Farmacologia Aplicada, Instituto de Tecnologia em Fármacos (Farmanguinhos), Fundação Oswaldo Cruz, Rio de Janeiro, Brazil.

[c] Instituto de Patologia Tropical e Saúde Pública (IPTSP), Universidade Federal de Goiás (UFG), Goiás, Goiânia, Brasil.

[d] Laboratório de Neurofisiologia, Departamento de Ciências Fisiológicas, Instituto de Biologia Roberto Alcantara Gomes, Universidade do Estado do Rio de Janeiro (UERJ), Rio de Janeiro, Brazil.

[e] Laboratório de Imunofarmacologia, Instituto Oswaldo Cruz (IOC), Fundação Oswaldo Cruz, Rio de Janeiro, Brazil.

[f] Laboratory of Endocrinology, Department of Endocrinology and Metabolism, Amsterdam University Medical Centers (UMC), University of Amsterdam, Amsterdam, The Netherlands.

[g] Laboratório de Farmacologia Celular e Molecular, Departamento de Biologia Celular; Instituto de Biologia Roberto Alcântara Gomes, Universidade do Estado do Rio de Janeiro (UERJ), Rio de Janeiro, Brazil.

[h] Departamento de Psicologia, Pontifícia Universidade Católica do Rio de Janeiro (PUC-Rio), Rio de Janeiro, Brazil.

[*]**Address correspondence to**: Dr. Carmen Penido, Laboratório de Farmacologia Aplicada, Departamento de Farmacologia Aplicada, Farmanguinhos, Fundação

Oswaldo Cruz, Rua Sizenando Nabuco 100, Manguinhos, Rio de Janeiro, RJ, CEP 21041-250, Brazil, e-mail: cpenido@gmail.com; carmen.penido@fiocruz.br.

Graphical Abstract

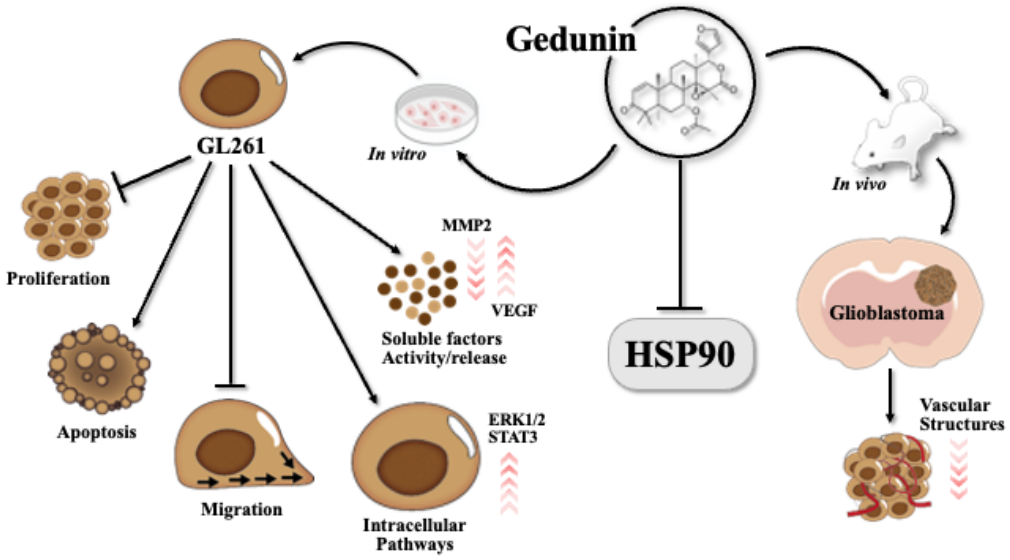

Highlights

- Gedunin reduces GL261 cell proliferation, migration and invasion *in vitro*.
- Gedunin induces GL261 cell apoptosis and ERK activation *in vitro*.
- Gedunin reduces the presence of tumoral vascular structures *in vivo*.

Abstract

Glioblastoma is the most invasive and malignant brain tumor, for which no effective treatment is currently available. Heat shock protein 90 (HSP90) is a potential target for the treatment of different types of cancer. Herein, we investigated the effect of gedunin, an HSP90 inhibitor, in murine GL261 glioblastoma *in vitro* and *in vivo* models. Gedunin treatment decreased GL261 cell proliferation and triggered apoptosis in a concentration-dependent manner. Gedunin also reduced GL261 cell migration and metalloproteinase-2 activity, suggesting that it impairs glioblastoma cell invasion.

Despite the reduction of total protein content in gedunin-treated cells, the phosphorylation of STAT3 and ERK1/2 pathways was enhanced within 24 h. *In situ* treatment with gedunin did not significantly reduce tumor volume, but reduced the presence of vascular structures in xenograft glioblastoma in C57BL/6 mice, a clinical feature associated with morbidity and mortality. Our results demonstrate that gedunin is a promising compound for the treatment of glioblastoma.

Keywords: Brain tumor, GL261, limonoids, natural products.

1. Introduction

Glioblastoma is a type of brain tumor that arises from phenotypically altered cells with neural stem cell-like properties [1]. This highly invasive and malignant tumor is defined by the World Health Organization as grade IV, based on histological, immunohistochemical, and molecular features [2]. Patients bearing glioblastoma have poor prognosis, with estimated median survival rates of eight months and a maximum five-year survival rate of only 5% [3,4].

The current standard protocol for glioblastoma treatment (Stupp protocol) relies on total tumor excision followed by high-dose radiotherapy with concurrent and adjuvant chemotherapy with temozolomide, a DNA alkylating agent [5]. The most common adverse events related to temozolomide treatment are myelosuppression (with cases of neutropenia, thrombocytopenia, lymphopenia, and anemia) and hepatotoxicity (affecting AST and ALT liver enzyme levels) [6–8]. Another limiting factor of glioblastoma treatment is that most orally and intravenously administered alkylating agents have poor blood-brain barrier permeability [9]. An alternative strategy is the usage of intracranial wafer implants containing the alkylating agent carmustine after tumor removal surgery, which, in combination with radiochemotherapy, has been shown to significantly improve patient survival [10,11]. However, carmustine wafers induce severe side effects, such as cerebral edema and hematological toxicity [6,12,13]. Another challenge in glioblastoma treatment with alkylating agents is the induction of resistance by the enhanced activity of the DNA-repair enzyme O6-methylguanine-DNA methyltransferase (MGMT) that repairs alkylating agents-induced DNA damage [14].

Glioblastoma is still considered incurable [15]; however, treatments targeting multiple signaling pathways are a promising strategy [16].

Modulation of the chaperone heat shock protein 90 (HSP90) is considered a potential antitumor therapy [17]. HSP90 activity is implicated on several hallmarks of cancer, such as proliferation, invasion, metastasis, angiogenesis, and resistance to apoptosis [18]. Increased expression of HSP90 correlates with tumor malignancy and poor prognosis in different types of cancer, including breast, colon, and melanoma [19–22]. Indeed, HSP90 chaperones several proteins involved in oncogenic processes, including the human epidermal growth factor receptor 2 (HER2/neu; ErbB2), tyrosine-protein kinase Src (Src), protein kinase B (AKT/PKB), breakpoint cluster region/Abelson murine leukemia virus (BCR/ABL) and tumor protein 53 (p53) [23–25]. In line with this, encouraging pre-clinical data have been obtained with HSP90 inhibitors in different types of tumor cells and animal models, including lymphoma, melanoma, breast, and lung cancer [26–30]. Currently, in the NIH´s Clinical Trials database ClinicalTrials.gov, there are more than a hundred registered trials (11 currently active) evaluating HSP90 inhibitors (alone or in combination with other drugs) for the treatment of different types of cancer [31]. Worthy of note, off-target toxicity, including ocular toxicity and hepatotoxicity, is a limiting factor for the use of these substances [32,33].

Over the past two decades, our group and others have been studying the antitumoral and anti-inflammatory effects of gedunin, a limonoid produced by vegetal species from the Meliaceae family [34] or by semi-synthetic routes [35]. Gedunin negatively modulates HSP90 activity by binding to the HSP90 co-chaperones p23 and cdc37 and, thus, impairing the formation of the active HSP90 complex [36,37]. This limonoid has potent antitumoral effects demonstrated against an array of tumor types *in vivo* and *in vitro* [36,38–41]. However, gedunin anti-tumoral effects have not been evaluated in glioblastoma.

Considering the urgent need for an effective therapy against glioblastoma and the high antitumor activity of the HSP90 inhibitor gedunin, here we investigate the antitumoral effect of this compound using the murine GL261 model both *in vitro* and *in vivo*.

126 **2. Materials and Methods**

127 ***2.1 Reagents and antibodies***

128 Gedunin (Gaia Chemicals, USA) and the specific HSP90 inhibitor 17-AAG (17-N-
129 allylamino-17-demethoxygeldanamycin, Tanespimycin, Sigma-Aldrich, USA) were
130 dissolved in DMSO (dimethyl sulfoxide, Sigma-Aldrich) and frozen at -86 °C until use.
131 MTT (3-(4,5-dimethylthiazol-2-yl)-2,5-diphenyl tetrazolium bromide), Dulbecco´s
132 modified Eagle´s medium (DMEM), phosphate buffer saline (PBS) tablet and trypsin-
133 EDTA (ethylenediamine tetraacetic acid) solution were purchased from Sigma Aldrich.
134 Fetal bovine serum (FBS) was purchased from Cultilab (Brazil). Propidium iodide (PI)
135 solution was obtained from Biolegend (USA). Vybrant™ CFDA-SE (carboxyfluorescein
136 diacetate succinimidyl ester) Cell Tracer Kit and gentamicin were obtained from
137 Thermo Fischer Scientific (USA). Annexin V-FITC (fluorescein isothiocyanate)
138 conjugated was purchased from BD Pharmingen (USA). IgG anti-mouse STAT3 (signal
139 transducer and activator of transcription 3, rabbit, C-20), anti-mouse-IgG-HRP
140 (horseradish peroxidase), and anti-rabbit-IgG-HRP secondary antibodies were
141 purchased from Santa Cruz Biotechnologies (USA). Antibodies against mouse p44/42
142 MAPK (mitogen-activated protein kinase, Thr202/Tyr204, D13.14.4E), ERK1/2
143 (extracellular signal-regulated kinase 1/2, rabbit), AKT (protein kinase B, PKB, rabbit,
144 pan, 40D4), phospho-AKT [rabbit, Ser473, (D9E)XP] and GAPDH (glyceraldehyde-3-
145 phosphate dehydrogenasemouse, D4C6R) were purchased from Cell Signaling (USA).
146 Antibodies against human PCNA (proliferating cell nuclear antigen, rabbit) were
147 purchased from Sino Biological (China). DNase I recombinant RNase free was
148 purchased from Roche Life Sciences (Germany).

149

150 ***2.2 GL261 cell culture and treatment***

151 Murine glioblastoma cell line (GL261, Cell Bank from Federal University of Rio de
152 Janeiro - UFRJ, Brazil) was cultured in DMEM (Sigma Aldrich) supplemented with 10
153 % FBS (Cultilab) and 50 µg/mL gentamicin (Thermo Fisher Scientific) in humidified
154 atmosphere (5 % CO_2 at 37 °C) until confluence. Cells were digested with 0.25 %
155 trypsin at the 5th passage and washed with 1x PBS. Cell viability was determined by
156 trypan blue (Sigma Aldrich) staining, under a light microscope, before further assays.

157 GL261 cells were incubated with 6.25-100 µM of gedunin for 24-72 h at 37 °C, 5 %
158 CO_2.
159
160 ***2.3 Animals***
161 Adult male C57BL/6 mice (20-25 g) provided by Oswaldo Cruz Foundation (Fiocruz)
162 breeding unit (Institute for Biomodels Science and Technology, Rio de Janeiro, Brazil)
163 were kept in standard autoclavable polypropylene boxes, with free access to food and
164 fresh water in environmentally controlled room temperature (ranging from 22 to 24 °C)
165 on a light/dark cycle at Farmanguinhos (Fiocruz, Rio de Janeiro, Brazil) and at the
166 Laboratory of Neurophysiology (State University of Rio de Janeiro, Rio de Janeiro,
167 Brazil) experimental animal facilities. Animal procedures were performed in accordance
168 with the ethical guidelines of the Brazilian National Council for the Control of Animal
169 Experimentation (CONCEA) and reported following the ARRIVE guidelines [42].
170 Experimental procedures were approved by the Ethics Commission on Animal Use of
171 Oswaldo Cruz Foundation (license #LW-35/16) and the Ethics Commission on Animal
172 Use of the State University of Rio de Janeiro (license #025/2017).
173
174 ***2.4 Primary mixed glial cell culture***
175 Under sterile conditions, mouse brain cortex tissue was rapidly dissected from
176 euthanized (150 mg/kg sodium thiopental, i.p.) young adult (4-week-old) C57BL/6 male
177 mice and transferred to ice-cold DMEM/F12 media (Sigma Aldrich) in 6 well plates.
178 After removal of the meninges, brain tissue was cut into small pieces, and washed three
179 times with 1x sterile PBS (Sigma Aldrich). Trypsin-DNAse solution (0.25 %-250
180 µg/mL) was added to the wells and the plate was incubated for 1 h in an orbital shaker
181 (Excella E24, New Brunswick Scientific, USA) at 37 °C and 150 rpm. Tissue samples
182 were vigorously triturated and dissociated with a 1 mL pipette tip. Cells were washed
183 with FBS-DNAse solution (10 %-250 µg/mL), added to a 20 % percoll gradient media,
184 and centrifuged at 800 × *g* for 30 min at 25 °C. Recovered cells were washed (400 × *g*,
185 10 min at 4 °C), distributed in T-25 bottle flasks, and incubated at 37 °C, 5 % CO_2.
186 DMEM/F12 media was changed every 3-4 days until use. Data were collected from two
187 independent experiments (n=5 mice per group; license #LW-35/16).
188

189 ***2.5 Proliferation assay***

190 GL261 cells (4 × 10^7/mL) were incubated with 5 μM CFSE solution (Invitrogen
191 Molecular Probes, USA) diluted in PBS for 15 min at 37 °C, 5 % CO_2. Cells were
192 washed with 10 % PBS/FBS solution, seeded in 24 well plates (2 × 10^5 cells per well),
193 incubated overnight, and treated with gedunin (6.25-100 μM) for 72 h. Cell proliferation
194 was evaluated by analyzing CFSE fluorescence intensity (FL1) upon cell divisions, by
195 flow cytometry (FACScalibur, Becton Dickinson, USA). Results were analyzed using
196 FlowJo X Software (Tree Star, Becton Dickinson).

197

198 ***2.6 MTT assay***

199 GL261 or primary mixed glial cells were seeded in a 96 flat bottom well plate (2 × 10^4
200 cells/well) and cultured in DMEM for 24 h (CO_2 5 % at 37 °C) for adhesion. Adherent
201 cells were cultured with different concentrations of gedunin (6.25-100 μM), 17-AAG (1
202 μM), or temozolomide (100 μM) for 20 or 68 h, when MTT solution (5 mg/mL; 22.5
203 μL/well) was added to the culture and incubated for 4 h. The analyzes were performed
204 at 24 and 72 h time points. Plates were centrifuged for 3 min (720 × *g* at 4 °C), the
205 supernatant was discharged and DMSO (150 μL/well) was added for formazan crystals
206 solubilization. The absorbance was read in a microplate reader (SpectraMax M5,
207 Molecular Devices, USA) at 540 nm.

208

209 ***2.7 Determination of apoptosis***

210 Apoptosis was evaluated using annexin V-FITC and propidium iodide (PI) staining.
211 GL261 cells were seeded in 24 well cell culture plates (2 ×10^5 cells/well) and left to
212 adhere overnight. GL261 cells were then incubated with gedunin (6.25 - 100 μM) for 24
213 or 72 h, followed by trypsinization, resuspension in annexin V Binding Buffer (HEPES
214 10 mM pH 7.4, NaCl 140 mM, $CaCl_2$ 2.5 mM) and labeling with annexin V-FITC and
215 PI for 15 min at room temperature. Cells incubated with medium were used as the
216 negative control, whereas 17-AAG-incubated cells were used as the positive control.
217 Staining was analyzed by cytometry using FACScalibur (Becton Dickinson) and
218 FlowJo Software (Tree Star, Becton Dickinson). At least 10^4 cells were acquired per
219 sample. Data are presented in dot plots in a log scale of increasing FL-1 (annexin V-
220 FITC) and FL-3 (PI) intensity.

221

222 ***2.8 Scratch assay***

223 GL261 cell monolayers, seeded into 6 well plates, were scratched at the center of the
224 well, and then the migration path was assessed at the leading edge of the scratch by
225 phase-contrast optical microscopy (100 ×, Olympus IX70, Japan) at indicated time
226 points. Analyses were performed by Image J software (National Institute of Health,
227 USA). The rate of migration was determined by quantifying the total distance that cells
228 moved from the edge of the scratch toward the center of the scratch, as previously
229 described [43].

230

231 ***2.9 Chemotaxis assay***

232 GL261 cell migration was assayed in a 48-well micro-chemotaxis Boyden chamber
233 (Neuro Probe Inc., USA). The bottom wells of the chamber were filled with DMEM 10
234 % FBS (29 μL) or serum-free DMEM media as the negative control. Polycarbonate
235 membrane filters with 8 μm pore size (Neuro Probe) were placed between the lower and
236 upper chambers. GL261 cells were pre-treated with different concentrations of gedunin
237 (6.25-25 μM) for 1 h in serum-free DMEM and then loaded into the upper wells of
238 Boyden chamber (2×10^4 cells/50 μL/well). The chamber was incubated in a humidified
239 atmosphere with 5 % CO_2 at 37 °C for 24 h. The membranes were removed and stained
240 using a Diff-quick (Laborclin, Brazil). The bottom side of membranes was visualized by
241 light microscopy for counting GL261 migrating cells (1000 ×, Olympus IX70). GL261
242 chemotaxis was calculated and expressed as the mean number of migrated cells in ten
243 random high-power fields (HPFs) per well (in quadruplicate).

244

245 ***2.10 Zymography***

246 GL261 cells were plated (1×10^6/well) in a 6-well plate in DMEM. After 24 h,
247 supernatant was removed, and cells were washed 3 times with pure DMEM to eliminate
248 any FBS trace. Then, cells received gedunin (6.25-50 μM) or 17-AAG (1 μM) treatment
249 in serum-free DMEM. After 48 h, the supernatant was collected and stored at -70 °C
250 until lyophilization. Samples were dehydrated in a Gamma 2-16 LSCplus (Christ,
251 Germany) ice condenser and, resuspended with 200 μL of zymography extraction buffer
252 (Tris-HCl 50 mM pH 7.5, NaCl 0.2 M, Triton X-100 0.1 %, $CaCl_2$ 10 mM, protease

253 inhibitor cocktail). Lowry method was used for protein quantitation. Enzymatic activity
254 of matrix metalloproteinase (MMP)-2 was determined on a 10 % SDS-PAGE
255 containing 0.1 % gelatin from porcine skin (Sigma Aldrich).
256
257 ***2.11 Enzyme-linked immunosorbent assay***
258 Levels of vascular endothelial growth factor (VEGF) were evaluated by sandwich
259 enzyme-linked immunosorbent assay (ELISA) in GL261 cell supernatants using
260 matched antibody pairs from R&D Systems (USA), according to the manufacturer's
261 instructions. Absorbance was determined by Spectramax M5 microplate reader
262 (Molecular Devices) at 490 nm.
263
264 ***2.12 Western blot***
265 GL261 cells (1×10^5 cells) treated with gedunin (6.25-100 μM) or 17-AAG (1 μM) for
266 24 h were lysed in a buffer containing protease inhibitors. Protein extract (20 μg) was
267 resolved by SDS-PAGE, proteins were transferred to polyvinylidene difluoride (PVDF)
268 membranes (GE Healthcare, USA), and then probed with primary antibodies.
269 Antibodies were diluted in Tris-buffered saline containing 0.5 % Tween 20 and 5 %
270 non-fat milk or bovine serum albumin (BSA, Sigma -Aldrich, USA), and incubated
271 overnight at 4 °C. On the following day, the membranes were incubated with
272 horseradish peroxidase (HRP)-conjugated secondary IgG (Santa Cruz Biotechnology)
273 for 1 h at room temperature. The blots were developed in a Hyperfilm with the use of a
274 chemiluminescent substrate (ECL Western blotting Detection Reagents; Amersham
275 Biosciences, USA). The band intensity was quantified using ImageJ (NIH, USA), and
276 expressed in arbitrary units (a.u.). The raw intensity values of total proteins were
277 normalized using the values of the control protein (PCNA) and of the control group
278 (untreated cells) to allow comparison between different experiments. The phospho-
279 protein values were normalized by the specific total-protein content.
280
281 ***2.13 Orthotopic glioblastoma model and osmotic mini-pump implantation***
282 Glioblastoma was induced in adult male C57BL/6 by stereotaxic injections of GL261
283 cells at the Laboratory of Neurophysiology experimental animal facility (UERJ, Rio de
284 Janeiro, Brazil). Mice were intraperitoneally anesthetized with 100 mg/kg ketamine

285 (Syntec, Brazil) and 10 mg/kg xylazine (Sedalex™ Venco, Brazil). Under sterile
286 conditions, a midline incision was made in the scalp, the skull was exposed to identify
287 bregma and lambda, and a small burr hole was drilled over the right hemisphere.
288 GL261 cells (5×10^4/μL; final volume of 2 μL) were stereotaxically injected into the
289 caudate putamen with a 10 μL Hamilton syringe at the rate of 0.5 μL/min. The needle
290 was slowly removed 4 min after the injection was finished. The following coordinates
291 (in mm) were used for stereotaxic injections (anterior-posterior; medial-lateral; dorsal-
292 ventral): 0.1 AP; 2.32 ML; 2.35 DV. Coordinates were based on the Cha et al., 2003
293 [44] descriptions and confirmed on Paxinos and Franklin mouse brain atlas [45].
294 Fourteen days after GL261 injections, animals were implanted with Alzet osmotic
295 minipumps (model 2004, 0.25 μL/h; Durect Corporation, USA) filled with gedunin
296 (250 μM, n=8) or DMSO (2.5 %, n=8). Cannulas (1-2 mm long) were placed into the
297 site of the tumor following similar surgical procedures described above. Treatment
298 lasted between 14 and 17 days. Mice were monitored every day for clinical signs of
299 pain and distress, such as ruffled fur, hunched back, trembling, convulsions, paralysis,
300 and permanent recumbency [46]. If signs of pain and distress were observed, the
301 animal was excluded from the study and euthanized. Data were collected from two
302 independent experiments (n=8 randomized mice per group). Mice were euthanized 28
303 days after GL261 injection with sodium thiopental (150 mg/kg, i.p.).
304
305 ***2.14 Mouse Brain Computed Tomography Images***
306 After 14-day treatment, anesthetized mice (100 mg/kg ketamine/10 mg/kg xylazine,
307 i.p.) were intravenously (i.v.) injected with 300 mg/mL of Omnipaque iohexol contrast
308 (GE Healthcare). Brains were scanned 3-6 min after contrast administration in a GE
309 Highspeed CT/E image system (Pedro Ernesto University Hospital, UERJ, Rio de
310 Janeiro, Brazil), according to the following protocol: 120 kV tube voltage, 55 mA, 1
311 mm slice thickness. Images were reconstructed in a 256 x 256-pixel matrix using
312 InVesalius 3.1.1 software (developed by Centro de Tecnologia da Informação Renato
313 Archer, CNPq, and Ministry of Health, Brazil). Tumor volumetry was determined by
314 selecting contrast-enhanced regions of interest in coronal sections.
315
316 ***2.15 Histology of Brain Tissue***

317 Euthanized mice (150 mg/kg sodium thiopental, i.p.) were perfused with 4%
318 formaldehyde. Mouse brains were collected and transferred into a 4 % formaldehyde
319 solution for 2 days for tissue fixation. Brains were then sectioned and embedded in
320 paraffin. Coronal sections of brain tissue (5 μm) were made using a Shandon Finesse
321 325 microtome (Thermo Fisher Scientific). Brain slices were stained with hematoxylin
322 (Merck, USA) and eosin (Sigma Aldrich, USA). Lesion size, liquefactive necrosis area,
323 vascular structures, intratumoral hemorrhage, and mitosis were blindly analyzed in the
324 central slice tumor area. Lesion size area was defined by the percentage of tumor area in
325 relation to the size of the brain area in the slice. The liquefactive necrosis area was
326 determined by the percentage of necrosis area in relation to the lesion size. Vascular
327 structures that had their full composition were counted in intratumoral and peritumoral
328 regions. Intratumoral hemorrhage was described in a semi-quantitative form regarding
329 the intensity at the slice, with the following definitions: discrete (+), moderate (++), and
330 intense (+++). Mitosis was characterized by estimating the average amount of cells per
331 analyzed field, and thus: >50% (+), 50-75% (++), and >75% (+++). Multipoint brain
332 slice images were composed in NIS-Elements AR (Nikon Corporation). Each brain slice
333 was analyzed by an observer blind to the experimental groups.
334
335 ***2.16 Statistical Analysis***
336 All analyzes were performed using GraphPad Prism 5 (GraphPad Software, USA).
337 Western blot analyzes were performed using the non-parametric Kruskal-Wallis test
338 followed by Dunn's multiple comparisons. Histologic analyzes were performed by one-
339 way analysis of variance (ANOVA) and Tukey's post-test for multiple comparisons. All
340 other comparisons were carried out using one-way ANOVA followed by Student-
341 Newman-Keuls test. Data are shown as the mean $\pm$ SEM (unless otherwise mentioned).
342 Significance was assumed either at the level of $p \leq 0.05$, $p \leq 0.01$, or $p \leq 0.001$, as
343 specified.
344

345 **3. Results**

346 ***3.1 Gedunin impairs GL261 cell growth and viability in vitro***

347 To verify the effect of gedunin on GL261 cell growth, a 72 h CFSE proliferation assay
348 was performed, in which staining decreases as cells proliferate. Incubation of CFDA-
349 SE-stained GL261 cells with gedunin decreased cell proliferation in a concentration-
350 dependent manner (**Fig. 1A**). Gedunin (25-100 μM) significantly inhibited GL261 cell
351 growth, similar to what was observed with the selective HSP90 inhibitor 17-AAG
352 (reference control). **Figure 1B** shows representative histograms of CFSE fluorescence
353 intensity (FL-1) of GL261 cells depicted in **Figure 1A**.

354 The effect of gedunin on cell viability was evaluated by the MTT assay. The incubation
355 of GL261 cells with gedunin decreased mitochondrial function in a concentration-
356 dependent manner within 24 and 72 h (**Fig. 1C**). MTT assay was also performed on
357 primary mixed glial cells to evaluate gedunin toxicity to non-tumoral cells. Gedunin
358 effect on primary mixed glial cells was less toxic, and higher concentrations were
359 required to induce cell death when compared to GL261 cells (**Fig. 1C**). The half-
360 maximal inhibitory concentration [IC50] of gedunin on GL261 cells was 2.3 times
361 lower than the IC_{50} observed on primary glial cells (**Fig. 1D**). Temozolomide, the first-
362 line treatment for glioblastoma, also reduced GL261 viability within 72 h in a
363 concentration-dependent manner (**Suppl. Fig. 1**). Considering the antiproliferative and
364 cytotoxic effects of gedunin on GL261 cells, we further examined whether this limonoid
365 induced apoptosis.

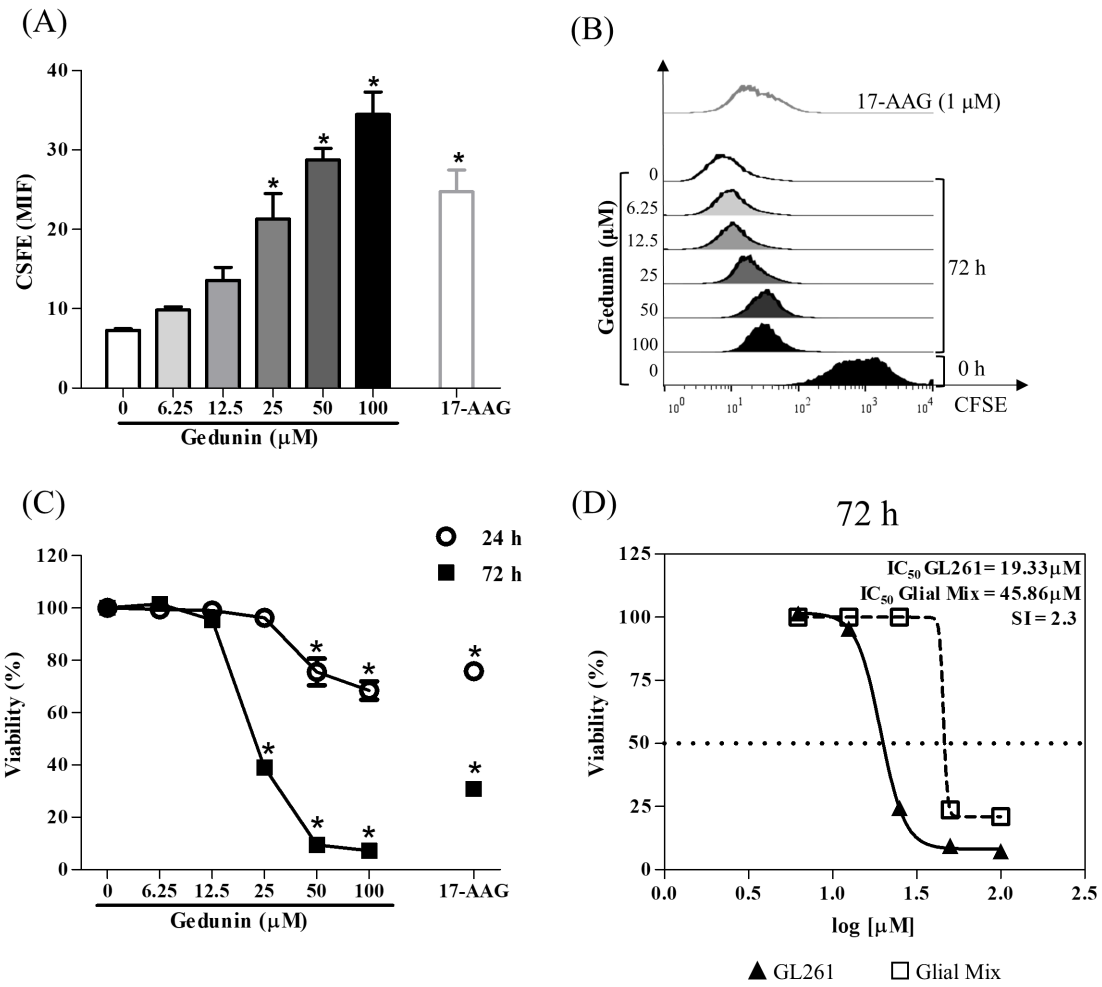

Figure 1. *Gedunin impairs GL261 cell proliferation.* (A) Effect of gedunin (6.25-100 μM) and 17-AAG (1 μM) on GL261 cell proliferation evaluated by CFSE staining and analyzed by FACScalibur (BD Biosciences) 72 h after incubation. Results are expressed as the mean ± SEM of median fluorescence intensity (MFI) from triplicate wells from three independent experiments. (B) Representative histogram shows CFSE fluorescence intensity (FL-1) from one experiment. (C) Effect of gedunin (6.25-100 μM) and 17-AAG (1 μM) on GL261 cell viability evaluated by MTT reduction assay (SpectraMax M5, Molecular Devices) 24 and 72 h after incubation. (D) IC50 values of gedunin treatment on GL261 and glial mixed cells 72 h after incubation. SI: selectivity index.

3.2 Gedunin induces GL261 cell apoptosis in vitro

Apoptosis is regulated by a series of signaling events that include disruption of the mitochondrial membrane and phosphatidylserine externalization [47,48]. Membrane phosphatidylserine staining by annexin V-FITC revealed that gedunin induced apoptosis of GL261 cells in a concentration- and time-dependent manner (**Fig. 2A**). Apoptosis was detected 24 h after treatment, and surpassed 90 % within 72 h, at the highest

383 concentrations. Representative dot plots of PI^+ and annexin V^+ cells are shown in
384 **Figure 2B**. Apoptotic cells are characterized by a reduced ability to scatter light either
385 in forward or right angle directions [49]. Indeed, GL261 cells incubated with gedunin
386 diminished FSC-H and increased SSC-H intensities, when compared to non-treated cells
387 (**Fig. 2C**). Representative dot-plots of the effect of 17-AAG (1 µM) on GL261 apoptosis
388 (24 h and 72 h) is available on **Supplemental Figure 2**.
389

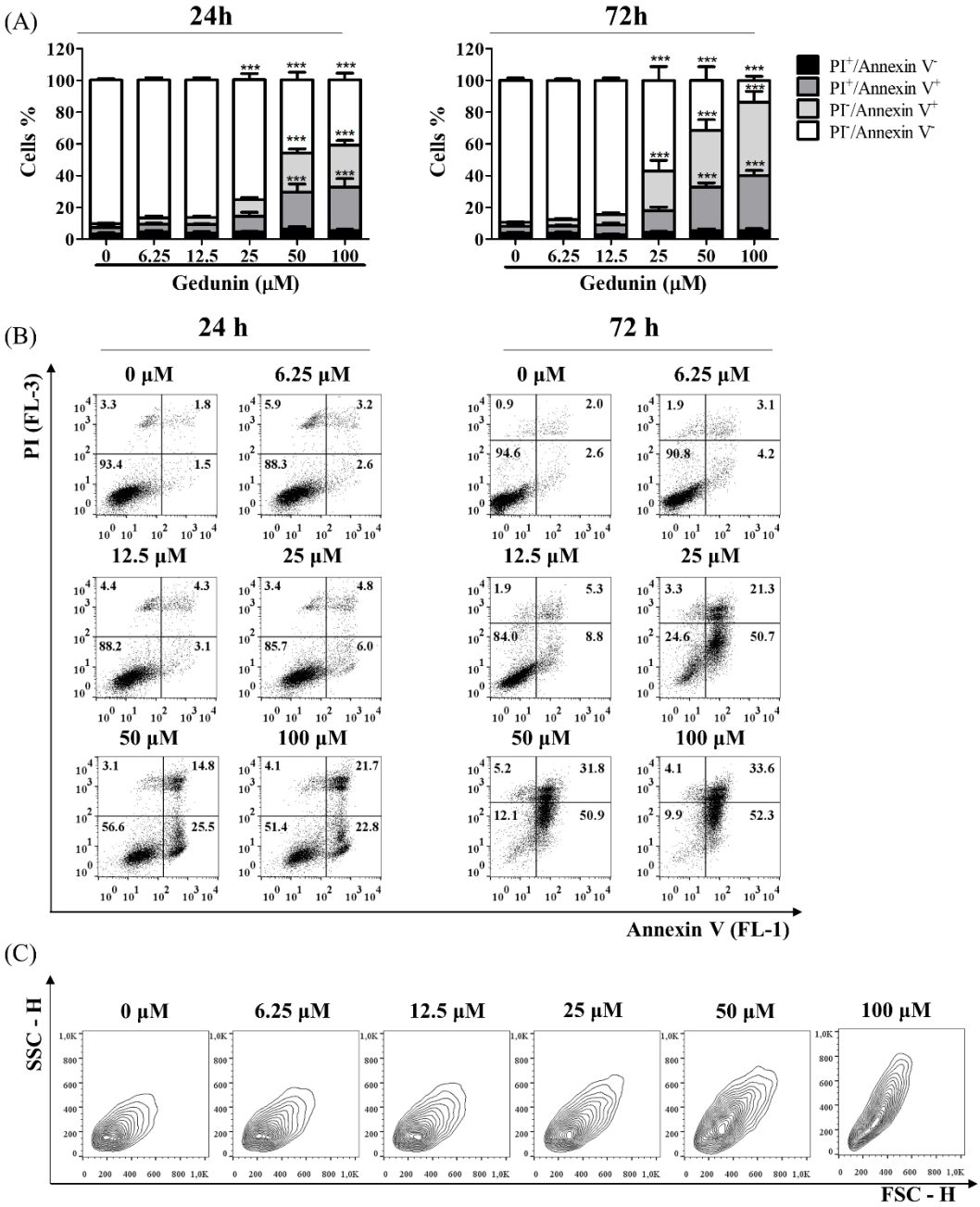

390

391 **Figure 2.** *Gedunin induces time- and concentration-dependent GL261 apoptosis.* (A) Effect of
392 gedunin (6.25-100 μM) on GL261 cell (2×10^4/well) apoptosis evaluated by propidium iodide
393 and annexin V-FITC staining MTT (FacsCalibur – BD Biosciences) 24 h and 72 h after
394 incubation. Results are expressed as the mean ± SEM of viability percentage from triplicates
395 wells from three independent experiments (24 well plates). * indicates statistically significant
396 differences ($p \leq 0.05$) between treated and untreated cells. (B) Representative dot plots of flow
397 cytometry analysis of gedunin-treated GL261 cells labeled with annexin V-FITC and PI after 24
398 and 72 h incubation. (C) Representative contour plots of SSC-H and FSC-H of gedunin-treated
399 (6.25 - 100 μM) GL261 cells after 72 h.
400

401 ***3.3 Gedunin impairs GL261 cell migration and invasiveness in vitro***

402 Tumor cell migration is an earlier step in cancer dissemination and invasion [50,51].
403 Scratch assay shows that gedunin (12.5 and 25 μM) reduced GL261 cell migration
404 when compared to the untreated group within 24 h, 48 h, and 72 h (**Fig. 3A, B**).
405 Confirming results obtained in the scratch assay, reduction of chemotaxis was also
406 observed in the Boyden chamber migration assay, in which gedunin treatment (25 μM)
407 impaired cell migration within 48 h (**Fig. 3C**).

408 Extracellular matrix remodeling by the proteolytic activity of tumor cell matrix
409 metalloproteinases (MMPs) is a crucial step for tumor cell invasion in the surrounding
410 tissue [52]. Gedunin also reduced the activity of MMP-2 (**Fig. 3D**), suggesting that this
411 limonoid impairs different mechanisms associated with tumor cell invasion. In addition,
412 we observed that gedunin treatment increased VEGF levels in the supernatant of GL261
413 cells (**Fig. 3E**), a phenomenon that does not contribute to its antitumoral effect since
414 pro-angiogenic mediators contribute to tumor cell metastasis [53,54].
415

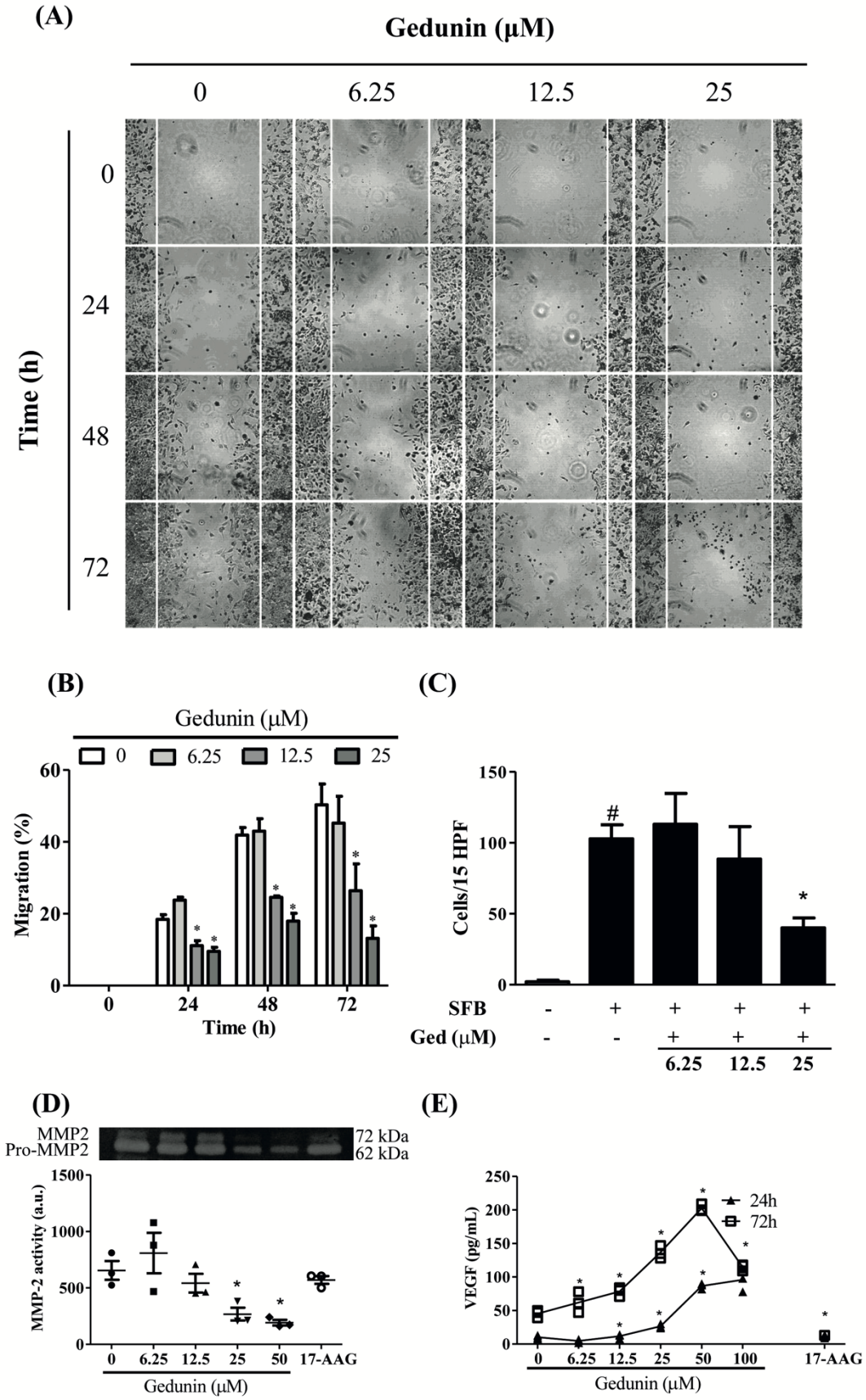
(A)
Gedunin (μM)
0
6.25
12.5
25
Time (h)
0
24
48
72
(B)
Gedunin (μM)
0
6.25
12.5
25
Migration (%)
Time (h)
(C)
Cells/15 HPF
SFB
Ged (μM)
6.25
12.5
25
(D)
MMP2
Pro-MMP2
72 kDa
62 kDa
MMP-2 activity (a.u.)
17-AAG
Gedunin (μM)
(E)
24h
72h
VEGF (pg/mL)
17-AAG
Gedunin (μM)

416

417 **Figure 3.** *Gedunin impairs in vitro GL261 cell migration and invasiveness.* (A) Microscopic
418 views of *in vitro* scratch assay. GL261 migration into the scratched area 24-72 h after gedunin
419 treatment (6.25-25 μM). (B) Percentages of GL261 cell migration calculated as the ratio of
420 uncovered area (24-72 h) by the initial scratched area (0 h). Results are expressed as the mean ±
421 SEM from two independent experiments (6 well plates). (C) Boyden chamber chemotaxis assay
422 demonstrating the number of gedunin-treated or untreated cells per 15 high power fields (HPF)
423 after 24 h migration. Results are expressed as the mean ± SEM from quadruplicate wells. (D)
424 MMP-2 activity of GL261 cell supernatant assessed by zymography assay 48 h after gedunin
425 treatment (6.25-50 μM). Results are expressed as the mean ± SEM from two independent
426 experiments. (E) VEGF quantification (ng/mL) in cell supernatant by ELISA assay 24 and 72 h
427 after gedunin treatment (6.25-100 μM). * indicates statistically significant differences ($p \leq 0.05$)
428 between treated and untreated cells, whereas # indicates statistically significant differences ($p \leq$
429 0.05) between stimulated and unstimulated cells.
430

431 ***3.4 Gedunin modulates signaling proteins in GL261 cells***

432 Genomic characterization of glioblastoma frequently shows amplification and
433 phosphorylation of RTK (receptor tyrosine kinase), which ultimately leads to its
434 autoactivation and downstream signaling pathways, resulting in constitutive cell
435 proliferation and resistance to apoptosis [55]. PI3K/AKT and Ras/ERK are the main
436 pro-survival pathways triggered by RTK activation in glioblastoma cells [56–58].
437 **Figure 4A-E** illustrates the effect of gedunin in these pathways in *in vitro*-treated
438 GL261 cells.

439 Gedunin treatment reduced the amount of total cell protein within 24 h, as shown in
440 representative immunoblots of proliferating cell nuclear antigen (PCNA) content from 8
441 independent experiments (**Fig. 4A**; **Suppl. Fig. 3**). Immunostaining of total proteins
442 also decreased in gedunin-treated cells (**Fig. 4A**), which may be explained by the
443 induction of apoptosis and cell death.

444 When the measurements were normalized by the constitutive protein, PCNA, no
445 specific reduction of total STAT3 or total ERK 1/2 was observed after gedunin
446 treatment (**Fig. 4B, C**). Total AKT protein content was reduced in GL261 cells treated
447 with gedunin (50 μM), when compared to untreated cell values (**Fig. 4D)**.

448 Phosphorylation of STAT3 (**Fig. 4E**) and ERK 1/2 (**Fig. 4F**) was induced by gedunin.
449 These results suggest that apoptosis driven by gedunin is followed by a compensatory
450 activation/phosphorylation of these survival pathways. The treatment with 17-AAG also
451 reduced total protein content but did not induce this putative compensatory activation of

452 STAT3 and ERK pathways within the 24 h incubation. Even though the mean of
453 phosphorylated AKT (pAKT) increased in gedunin-treated cells (**Fig. 4C**), it was not
454 significantly different from untreated cells (**Fig. 4G**).

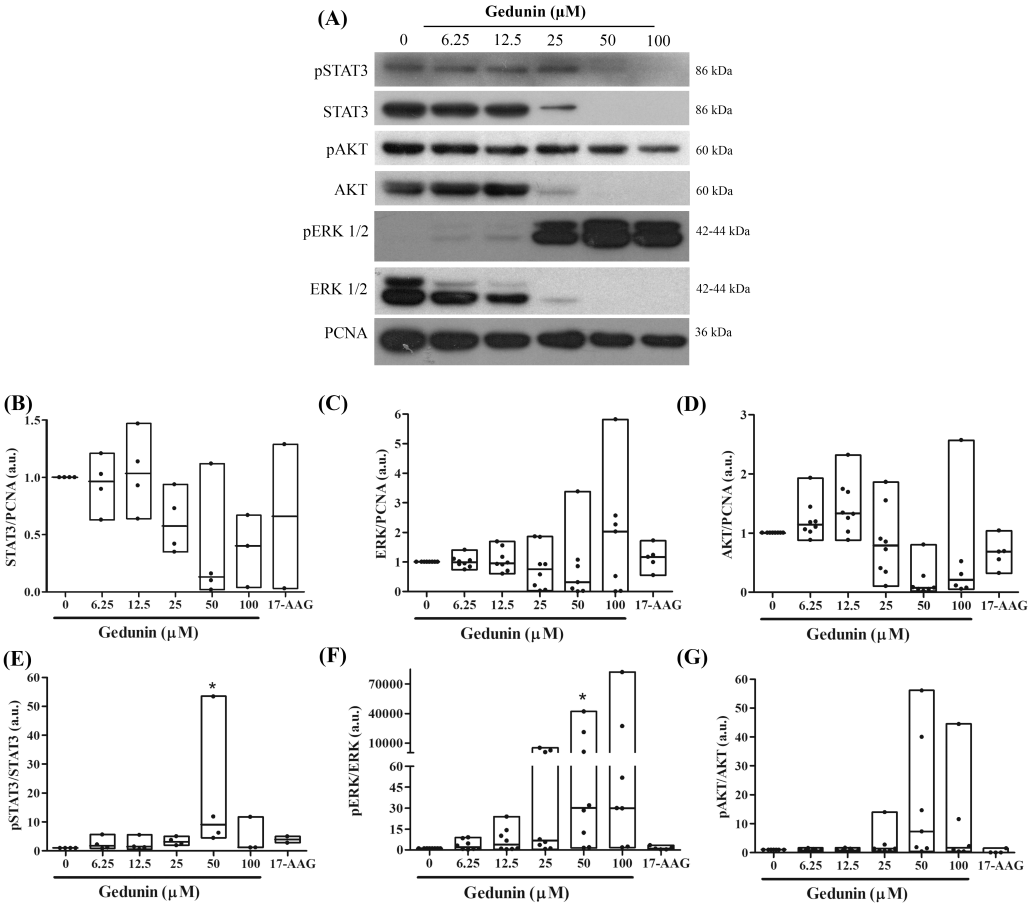

455

456 **Figure 4.** *Gedunin activates PI3K/AKT and STAT3/ERK 1/2 pathways.* Western blot analysis of
457 the effect of gedunin (6.25 – 100 μM) on intracellular signaling proteins, 24 h after treatment.
458 (A) Representative immunoblots of one experiment out of 8 independent experiments with a
459 similar trend. Box plots of (B) STAT3/PCNA, (C) ERK/PCNA, (D) AKT/PCNA, (E)
460 pSTAT3/STAT3, (F) pERK/ERK, (G) pAKT/AKT intracellular signaling pathways on GL261
461 cells. 17-AAG was used as the reference control of HSP90 activity inhibition. PCNA was used
462 as the loading control. Results are expressed as the mean ± SEM of protein expression from
463 eight independent experiments. * indicates statistically significant differences ($p \leq 0.05$)
464 between treated and untreated cells, whereas # indicates statistically significant differences ($p \leq$
465 0.05) between stimulated and unstimulated cells.
466

467 ***3.5 Gedunin effect on glioblastoma in vivo***

468 The orthotopic C57BL/6 mouse glioblastoma model used in the present study has been
469 established as a standard procedure to reproduce human molecular and histological

features of glioblastoma [59,60]. Biodistribution data obtained by our group show that ^{99m}Tc-labeled-gedunin did not reach substantial levels in the brain tissue when intravenously injected in mice (Costa et al., *manuscript in preparation*). We, therefore, assessed whether gedunin *in vivo* treatment was effective by using osmotic pumps placed *in situ.*

Computed tomography (CT) scans revealed solid tumor growth that occupied an extensive area of the brain tissue of mice from all groups (white mass, top panels in black background of **Fig. 5A,** indicated by an asterisk in the upper left image scan). Three-dimensional reconstructions of CT images are shown in **Figure 5** bottom panels, in which tumor mass is represented by white over gray (brain) areas. Even though tumor volume median values (mm^3) of gedunin-treated mice were smaller than those for untreated or DMSO-injected mice, variability within groups was high (lowest and highest tumor volume values for each group were: untreated, 21.7 - 75.6; DMSO, 16.8 - 83.6; Ged, 11.7 - 67.4). No significant differences were observed between groups (ANOVA, p = 0.106; **Fig. 5B, C**). **Supplemental Figure 4** shows CT of mouse brains with and without tumors, for a better illustration of the tumor mass. Body mass (g) was measured before GL261 injection and 28 days later and no alterations were observed (data not shown).

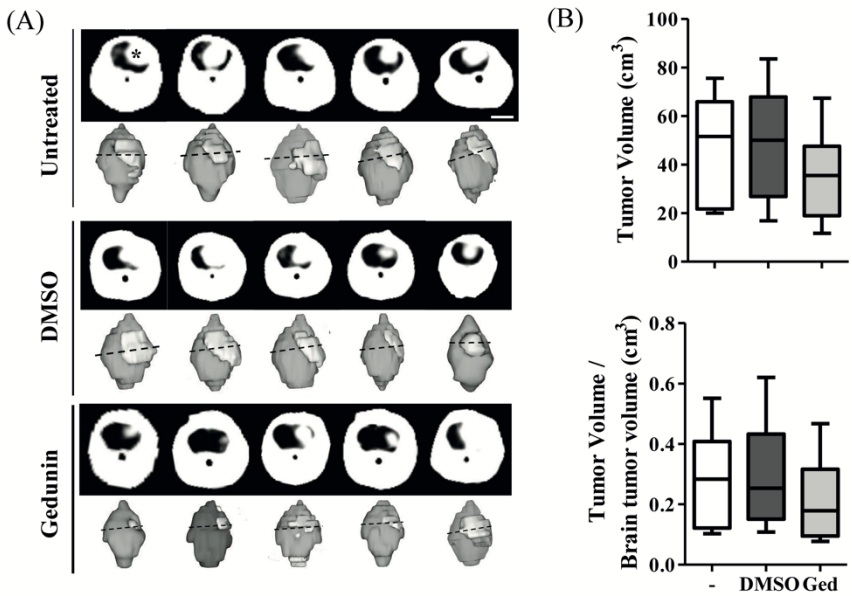

Figure 5. *Brain CT analysis of gedunin-treated mice.* (A) Representative sequential coronal CT-images and respective 3D brain reconstructions (dorsal view) from untreated, DMSO-injected

491 and gedunin (250 μM)-treated mice. Lighter regions in 3D reconstructions represent brain
492 tumors. Images were acquired after 14-day *in situ* treatment (Alzet® osmotic minipumps) in
493 GL261 cell-injected mice (1× 10^5 cells/brain/2 μL). Boxplot graphs show the ratio between
494 tumor and mouse brain volume values (B) and tumor volume values (C) from 6-8 mice per
495 group out of 2 independent experiments. Tumor volumetry was determined by selecting
496 contrast-enhanced regions of interest in coronal sections using InVesalius 3.1.1 software. CT:
497 computed tomography. *White area corresponds to glioblastoma observed in all CT scans.
498 Dashed line: coronal slice cut point.
499

500 Histological examination of coronal brain sections of untreated, DMSO- and gedunin-
501 treated groups revealed that even though gedunin-treated mice had larger tumor-
502 induced lesion areas, they displayed reduced vascular structures (**Table 1**). Areas of
503 liquefactive necrosis, intratumoral hemorrhage, and mitosis were not statistically
504 different between groups. **Figure 6** depicts representative images of GL261-injected
505 mouse coronal brain slices stained with hematoxylin and eosin 28 days after injections.
506 **Figure 6 (A-C)** insets represent 400× magnification of intratumoral perinecrotic
507 regions, in which liquefactive necrosis can be observed by white spaces within the
508 glioblastoma tissue, resulting in the loss of tissue architecture. **Figure 6 (D-F)** displays
509 1000 × magnification of representative images of tumor tissue showing mitosis,
510 characterized by tumor cell proliferation, and areas of hemorrhage, defined by the
511 presence of red blood cells.
512
513 **Table 1**. **Glioblastoma histology features after gedunin *in vivo* treatment**

	Untreated	DMSO	Gedunin	p
Lesion size	27%	45%	45.2%	NS
Vascular Structures	13	32	8	P< 0.05 *
Liquefactive Necrosis	9.6%	10.6%	8.8%	NS
Intratumoral Hemorrhage	+	++	++	NS
Mitosis	+	++	+	NS

514 **Table 1**. *Glioblastoma histology features after gedunin in vivo treatment.* Table shows absolute
515 and semi-quantitative description of the histological analyses of brain slices and p-values of
516 gedunin-treated vs DMSO-treated mice, analyzed by Tukey's post-test. NS= non-significant; +=
517 discrete; ++= moderate.
518

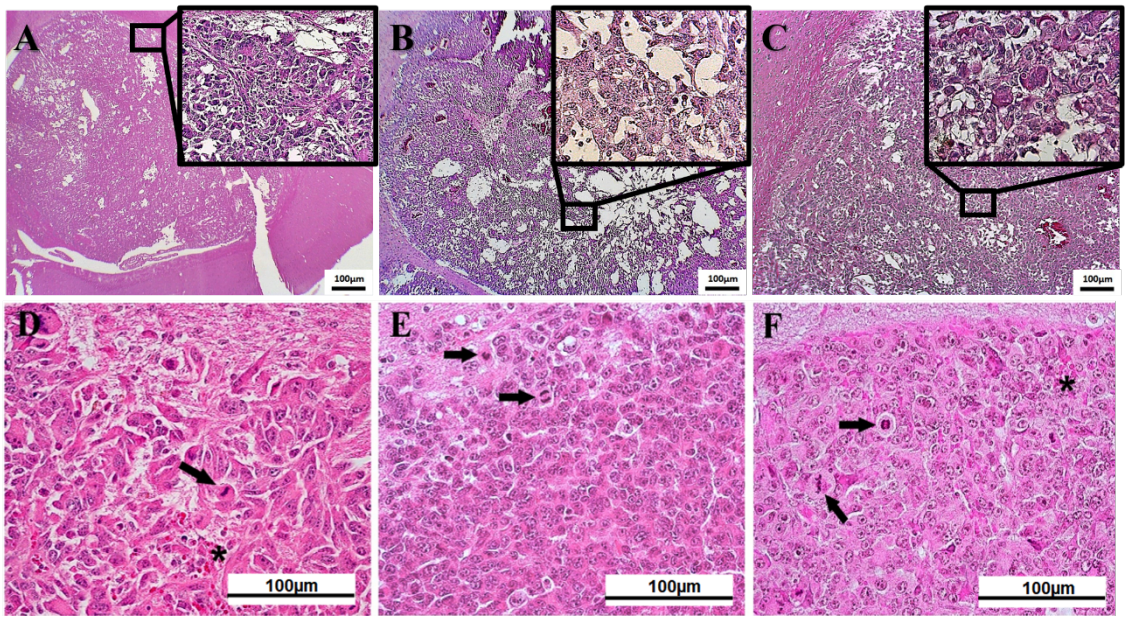

Figure 6. *Histological analysis of gedunin-treated mice.* Representative images of coronal brain slices from stained with hematoxylin and eosin 28 days after GL261 cell implantation of untreated (A,D), DMSO- (B,E), and gedunin-treated (C,F) mice (n=8 per group). Upper panels (A-C) depict low magnification images (40 ×) of the extent of the tumor area for each experimental group. Corresponding high-magnification insets (400 ×) of intratumoral perinecrotic regions show liquefactive necrosis (white regions). Lower panels (D-F), high magnification images (1000 ×) from the same animals in (A-C), show mitosis (black arrows) and areas of hemorrhage (asterisks) in intratumoral regions.

4. Discussion

Uncontrolled proliferation and apoptosis resistance are central features of tumor development, being major targets for cancer treatment [18]. HSP90 is a key factor for tumor growth, since it chaperones several essential proteins involved in oncogenic processes. In the present study, we demonstrate that gedunin, a natural occurring HSP90 inhibitor, impairs glioblastoma cell growth *in vitro*, by arresting proliferation and inducing cell death in non-toxic concentrations to primary brain cells. Gedunin also reduced glioblastoma cell migration, tumor-related signaling pathways, and extracellular metalloproteinase MMP-2 activity, features involved in glioblastoma growth. GL261-orthotopically injected C57BL/6 mice treated with gedunin showed reduced presence of vascular structures, even though no changes were observed in tumor-size.

Data shown in **Supplemental Figure 5** supports previous knowledge that both gedunin and other HSP90-binding agents induce the expression of HSP70 in cancer cells due to

543 HSP90 inhibition [61–63]. The antiproliferative and cytotoxic effects of gedunin on
544 GL261 cells are also in accordance with previous *in vitro* results showing similar
545 antitumoral effects of gedunin against different cell lines [36,38–41]. Worthy of note,
546 gedunin toxicity against GL261 cells was achieved at a concentration lower than half
547 the one required to affect primary glial cells, with a selectivity index of 2.3 [64]. This
548 might be explained by the increased affinity of HSP90 inhibitors to HSP90 machinery
549 expressed by tumor cells [17], or by biological and metabolic differences between
550 primary and glioblastoma cells [65]. Gedunin-triggered apoptosis, detected by
551 phosphatidylserine exposure on the cell surface, was confirmed by flow cytometric
552 analysis of cell physical criteria that showed the reduced size and increased granularity
553 of apoptotic cells, due to the formation of apoptotic bodies and plasma membrane
554 blebbing [49]. Our results clearly show that, as apoptosis progresses, GL261 cell FSC
555 becomes progressively lower, likely due to cell dehydration and shrinkage. On the other
556 hand, enhancement of SSC occurs due to cytoplasm and nuclear condensation [49,66].

557 Glioblastoma is a highly invasive and diffuse tumor that requires cell migration and
558 extracellular matrix degradation to spread to adjacent tissue [67,68]. Scratch and
559 chemotaxis assays showed that gedunin diminished GL261 migration, in concentrations
560 and time points lower than the ones that induced cytotoxicity. Another way by which
561 gedunin controls tumor invasiveness is by inhibiting MMP-2 activity, with a higher
562 effect than 17-AAG. Indeed, it has been shown that HSP90 stabilizes and promotes the
563 activation of extracellular MMP-2, being crucial for GL261 and HT-1080 tumor cell
564 invasion [69,70].

565 Our results show that gedunin induced a reduction of total protein in GL261 cells,
566 which is compatible with the HSP90 inhibition. PI3K/AKT and STAT3 are signaling
567 pathways that function as pro-survival factors in a wide range of primary tumors,
568 including glioblastoma [56,71]. Reduced expression of total PI3K and AKT by gedunin
569 suggests that this limonoid impairs either PI3K/AKT network or an upstream protein,
570 such as epithelial growth factor receptor (EGFR). In accordance, it has been shown that
571 gedunin also impaired the PI3K/AKT/mTOR pathway in *in vivo* models of hamster oral
572 carcinoma [41] and murine pancreatic cancer [38]. Even though PI3K/AKT is the
573 preferential signaling pathway in glioblastoma, it has been reported that glioblastoma
574 cells are not exclusively dependent on this pathway and that PI3K/AKT/mTOR-specific

575 inhibitors might not be effective against this brain tumor [56]. Hence, we evaluated the
576 effect of gedunin in AKT, ERK 1/2, and STAT3 signaling, which are also altered in
577 glioblastoma cells and are involved in the cell cycle [72,73]. It is important to note that
578 even though gedunin treatment reduced total ERK content, it did not inhibit ERK1/2
579 phosphorylation. On the contrary, ERK was strongly phosphorylated/activated in cells
580 treated with gedunin. Indeed, Duron et al. showed that HSP90 inhibition can also
581 prompt the phosphorylation/activation of ERK [74,75]. There might be a compensatory
582 survival mechanism in GL261 cells that activate ERK when HSP90 is inhibited. This
583 result must be further explored and points to the perspective of combining gedunin with
584 ERK inhibitor anti-tumoral drugs.

585 It has been previously reported in glioblastoma that constitutive activation of STAT3
586 results from the fusion of the RTK epidermal growth factor receptor (EGFR) with the
587 GTP-binding protein Septin 14 (SEPT14) [58]. STAT3 signaling promotes glioblastoma
588 cell survival, and suppresses apoptosis [58]. Abnormal STAT3 activation in
589 glioblastoma is correlated with the control of several events involved in tumor growth
590 [71]. The late (24 h) activation of STAT3 by gedunin might also correspond to survival
591 feedback following the induction of apoptosis. Therefore, gedunin may inhibit GL261
592 cell proliferation by acting on different pathways that induce apoptosis. Activation of
593 STAT3 is required for VEGF production [76,77]. Even though we observed that
594 gedunin impaired signaling pathways (which was expected to impair both VEGF
595 synthesis and signaling pathway), this phenomenon did not inhibit VEGF release by
596 GL261 *in vitro*.

597 As previously mentioned in the results section, even though our findings indicate that
598 gedunin fits the predicted ADMET criteria for druggability and BBB permeation,
599 systemic (i.v.) administration of ^{99m}TC-labeled gedunin failed to reach the brain tissue
600 at substantial levels (Costa *et al*., manuscript in preparation). Hence, we used gedunin-
601 filled Alzet® minipumps to perform *in situ* treatment (resembling the FDA-approved
602 Gliadel® [carmustine] implants) to ensure that gedunin would be available at the tumor
603 site. It is important to note that the residual volume of gedunin inside the minipumps
604 was measured at the end of treatment to ensure that gedunin was released *in situ*, (values
605 shown in **Suppl. Table 1**). We observed that the number of mice bearing reduced-
606 volume tumors was higher in gedunin-treated group when compared to DMSO-treated

607 group, even though this treatment did not significantly reduce tumor volumes detected
608 by CT imaging. Regarding our CT imaging results, it is important to emphasize the
609 limitation of the technique, since the limited spatial resolution of clinical CT scanners
610 might not be precise to analyze such a small brain [78,79]. While our findings reinforce
611 the feasibility of using clinical CT scanners for *in vivo* brain tumor imaging in mice,
612 their use for detecting treatment responses in tumor volume requires further
613 investigation, since clinical CT scans are made for imaging humans that have brain
614 volumes roughly 3,000 times greater than mice [80–82]. Another limitation is that
615 mouse tumor sizes were not evaluated over the days, since CT scan was only feasible in
616 mice with no minipump implants, due to the stainless steel of brain infusion cannulas.
617 As expected, GL261-injections triggered the development of mouse glioblastoma in
618 orthotopically-injected C57BL/6 mouse with liquefactive necrosis, hemorrhage,
619 mitosis and increased vascular structures [59]. *In situ* treatment with gedunin reduced
620 the presence of vascular structures, which might decrease tumor nutritional supply.
621 Considering that gedunin increased the production of VEGF *in vitro*, this finding might
622 suggest that gedunin impairs angiogenesis in GL261 tumors by a mechanism
623 independent of VEGF *in vivo* as previously described [83]. Despite the reduction of
624 vascular structures, there was no evidence of reduction in tumor size. Moreover, the
625 impact of the reduction in vascular structures on the survival rate of orthotopically-
626 injected C57BL/6 mice was not evaluated. Therefore, whether gedunin *in vivo*
627 treatment impairs mouse glioblastoma growth needs to be further investigated,
628 including *in situ* measurement of gedunin release from minipumps and VEGF contents.
629 Noteworthy, both DMSO- and gedunin-treated mice showed increased lesion areas
630 when compared to untreated mice, which might be a consequence of the surgical
631 procedure required for minipump implantation. It is possible that an optimized
632 treatment protocol including a postoperative treatment (as generally performed in
633 glioblastoma patients) and/or association with other drugs result in a better outcome.

634 The severity and the poor prognosis of patients bearing glioblastoma urge for new
635 therapeutical targets and drugs. Data presented in this paper sheds light on alternative
636 treatments for this type of tumor by revealing GL261 dependency of HSP90 and
637 gedunin as a potential lead compound.
638

639 ***Author contributions***

640 CP, TEMMC, and TEK conceived and designed the work. TEMMC, CP, TEK, ACM,
641 and MGH designed experiments. TEMMC, TAP, LNS, EMC, CCF, CMMM, JXP,
642 VGR, and TEK performed the experiments, acquired, and/or analyzed data. CP, TEK,
643 ACM, YAV, JXC, and MGH contributed with funding and resources. CP supervised the
644 work. CP and TEMMC wrote the original draft. CMMM and TEK wrote and revised
645 the manuscript. All authors revised and edited the final manuscript.

646

647 ***Acknowledgments***

648 The authors gratefully acknowledge Dr. André Luis Peixoto Candéa, D.Sc. Erika
649 Tatiana Muñoz, Dr. Samara Cristina Ferreira Machado, Edson Santos Silva, Filipe Leal
650 Portilho, Ubirajara Ribeiro, and Maria Heloisa Oliveira for technical support. We also
651 thank the Institute for Biomodels Science and Technology (Fiocruz) for providing mice,
652 and the Center for Cancer Control (CUCC, UERJ) for the help with CT imaging
653 acquisition.

654

655 ***Funding***

656 This work was supported by the Carlos Chagas Filho Research Support Foundation
657 (FAPERJ), the Coordination for the Improvement of Higher Education Personnel
658 (CAPES), the Brazilian agency National Council for Scientific and Technological
659 Development (CNPq), and the Oswaldo Cruz Foundation (Fiocruz). CP, MGMO, and
660 ACM hold fellowships from CNPq. TEMMC was a PhD student from the Graduate
661 Program in Cell and Molecular Biology (IOC/Fiocruz).

662

663 ***Conflict of interest***

664 The authors declare no conflict of interest.

665

666 ***References***

667 [1] H.S. Phillips, S. Kharbanda, R. Chen, W.F. Forrest, R.H. Soriano, T.D. Wu, A.
668 Misra, J.M. Nigro, H. Colman, L. Soroceanu, P.M. Williams, Z. Modrusan, B.G.

669 Feuerstein, K. Aldape, Molecular subclasses of high-grade glioma predict
670 prognosis, delineate a pattern of disease progression, and resemble stages in
671 neurogenesis, Cancer Cell. 9 (2006) 157–173. doi:10.1016/J.CCR.2006.02.019.

672 [2] D.N. Louis, A. Perry, G. Reifenberger, A. von Deimling, D. Figarella-Branger,
673 W.K. Cavenee, H. Ohgaki, O.D. Wiestler, P. Kleihues, D.W. Ellison, The 2016
674 World Health Organization Classification of Tumors of the Central Nervous
675 System: a summary, Acta Neuropathol. 131 (2016) 803–820.
676 doi:10.1007/s00401-016-1545-1.

677 [3] Q.T. Ostrom, M. Price, C. Neff, G. Cioffi, K.A. Waite, C. Kruchko, J.S.
678 Barnholtz-Sloan, CBTRUS Statistical Report: Primary Brain and Other Central
679 Nervous System Tumors Diagnosed in the United States in 2015–2019, Neuro.
680 Oncol. 24 (2022) v1–v95. doi:10.1093/neuonc/noac202.

681 [4] P.D. Delgado-López, E.M. Corrales-García, Survival in glioblastoma: a review
682 on the impact of treatment modalities, Clin Transl Oncol. 18 (2016) 1062–1071.
683 doi:10.1007/s12094-016-1497-x.

684 [5] R. Stupp, W.P. Mason, M.J. van den Bent, M. Weller, B. Fisher, M.J. Taphoorn,
685 K. Belanger, A.A. Brandes, C. Marosi, U. Bogdahn, J. Curschmann, R.C. Janzer,
686 S.K. Ludwin, T. Gorlia, A. Allgeier, D. Lacombe, J.G. Cairncross, E. Eisenhauer,
687 R.O. Mirimanoff, E.O. for R. Groups, T. of Cancer Brain Tumor, Radiotherapy,
688 N.C.I. of C.C.T. Group, Radiotherapy plus concomitant and adjuvant
689 temozolomide for glioblastoma, N Engl J Med. 352 (2005) 987–996.
690 doi:10.1056/NEJMoa043330.

691 [6] M. Niewald, C. Berdel, J. Fleckenstein, N. Licht, R. Ketter, C. Rübe, Toxicity
692 after radiochemotherapy for glioblastoma using temozolomide - a retrospective
693 evaluation, Radiat. Oncol. 6 (2011) 141. doi:10.1186/1748-717X-6-141.

694 [7] J. Dinnes, C. Cave, S. Huang, R. Milne, A rapid and systematic review of the
695 effectiveness of temozolomide for the treatment of recurrent malignant glioma,
696 Br. J. Cancer. 86 (2002) 501–505. doi:10.1038/sj.bjc.6600135.

697 [8] F. Attarian, F. Taghizadeh-Hesary, A. Fanipakdel, S.A. Javadinia, P. Porouhan,
698 B. PeyroShabany, D. Fazilat-Panah, A Systematic Review and Meta-Analysis on
699 the Number of Adjuvant Temozolomide Cycles in Newly Diagnosed
700 Glioblastoma, Front. Oncol. 11 (2021) 1–6. doi:10.3389/fonc.2021.779491.

[9] L. Jena, E. McErlean, H. McCarthy, Delivery across the blood-brain barrier: nanomedicine for glioblastoma multiforme, Drug Deliv. Transl. Res. 10 (2020) 304–318. doi:10.1007/s13346-019-00679-2.

[10] M.J. McGirt, K.D. Than, J.D. Weingart, K.L. Chaichana, F.J. Attenello, A. Olivi, J. Laterra, L.R. Kleinberg, S.A. Grossman, H. Brem, A. Quiñones-Hinojosa, Gliadel (BCNU) wafer plus concomitant temozolomide therapy after primary resection of glioblastoma multiforme, J. Neurosurg. JNS. 110 (2009) 583–588. doi:10.3171/2008.5.17557.

[11] Z. Qi, W. Xing, C. Shao, C. Yang, Z. Wang, The role of Gliadel wafers in the treatment of newly diagnosed GBM: a meta-analysis, Drug Des. Devel. Ther. 9 (2015) 3341. doi:10.2147/DDDT.S85943.

[12] T. Reithmeier, E. Graf, T. Piroth, M. Trippel, M.O. Pinsker, G. Nikkhah, BCNU for recurrent glioblastoma multiforme: efficacy, toxicity and prognostic factors, BMC Cancer. 10 (2010) 30. doi:10.1186/1471-2407-10-30.

[13] A. Bregy, A.H. Shah, M. V Diaz, H.E. Pierce, P.L. Ames, D. Diaz, R.J. Komotar, The role of Gliadel wafers in the treatment of high-grade gliomas, Expert Rev. Anticancer Ther. 13 (2013) 1453–1461. doi:10.1586/14737140.2013.840090.

[14] E. Lechapt-Zalcman, G. Levallet, A.E. Dugué, A. Vital, M.-D. Diebold, P. Menei, P. Colin, P. Peruzzy, E. Emery, M. Bernaudin, F. Chapon, J.-S. Guillamo, O6-methylguanine-DNA methyltransferase (MGMT) promoter methylation and low MGMT-encoded protein expression as prognostic markers in glioblastoma patients treated with biodegradable carmustine wafer implants after initial surgery followed by radiotherapy w, Cancer. 118 (2012) 4545–4554. doi:https://doi.org/10.1002/cncr.27441.

[15] O. Alexandru, S. Purcaru, L. Tataranu, L. Lucan, J. Castro, C. Folcuţi, S.-A. Artene, C. Tuţă, A. Dricu, The Influence of EGFR Inactivation on the Radiation Response in High Grade Glioma, Int. J. Mol. Sci. 19 (2018) 229. doi:10.3390/ijms19010229.

[16] S. Tanaka, D.N. Louis, W.T. Curry, T.T. Batchelor, J. Dietrich, Diagnostic and therapeutic avenues for glioblastoma: no longer a dead end?, Nat. Rev. Clin. Oncol. 10 (2013) 14–26. doi:10.1038/nrclinonc.2012.204.

[17] J. Trepel, M. Mollapour, G. Giaccone, L. Neckers, Targeting the dynamic HSP90

733 complex in cancer, Nat Rev Cancer. 10 (2010) 537–549. doi:10.1038/nrc2887.
734 [18] D. Hanahan, R.A. Weinberg, Hallmarks of cancer: the next generation, Cell. 144
735 (2011) 646–674. doi:10.1016/j.cell.2011.02.013.
736 [19] Q. Cheng, J.T. Chang, J. Geradts, L.M. Neckers, T. Haystead, N.L. Spector, H.K.
737 Lyerly, Amplification and high-level expression of heat shock protein 90 marks
738 aggressive phenotypes of human epidermal growth factor receptor 2 negative
739 breast cancer, Breast Cancer Res. 14 (2012) R62. doi:10.1186/bcr3168.
740 [20] H. Kubota, S. Yamamoto, E. Itoh, Y. Abe, A. Nakamura, Y. Izumi, H. Okada, M.
741 Iida, H. Nanjo, H. Itoh, Y. Yamamoto, Increased expression of co-chaperone
742 HOP with HSP90 and HSC70 and complex formation in human colonic
743 carcinoma, Cell Stress Chaperones. 15 (2010) 1003–1011. doi:10.1007/s12192-
744 010-0211-0.
745 [21] M.M. McCarthy, E. Pick, Y. Kluger, B. Gould-Rothberg, R. Lazova, R.L. Camp,
746 D.L. Rimm, H.M. Kluger, HSP90 as a marker of progression in melanoma, Ann
747 Oncol. 19 (2008) 590–594. doi:10.1093/annonc/mdm545.
748 [22] E. Pick, Y. Kluger, J.M. Giltnane, C. Moeder, R.L. Camp, D.L. Rimm, H.M.
749 Kluger, High HSP90 expression is associated with decreased survival in breast
750 cancer, Cancer Res. 67 (2007) 2932–2937. doi:10.1158/0008-5472.CAN-06-
751 4511.
752 [23] F.H. Schopf, M.M. Biebl, J. Buchner, The HSP90 chaperone machinery, Nat Rev
753 Mol Cell Biol. 18 (2017) 345–360. doi:10.1038/nrm.2017.20.
754 [24] Y. Fukuyo, C.R. Hunt, N. Horikoshi, Geldanamycin and its anti-cancer activities,
755 Cancer Lett. 290 (2010) 24–35. doi:10.1016/j.canlet.2009.07.010.
756 [25] M. V Blagosklonny, Hsp-90-associated oncoproteins: multiple targets of
757 geldanamycin and its analogs, Leukemia. 16 (2002) 455–462.
758 doi:10.1038/sj.leu.2402415.
759 [26] N. Gaspar, S.Y. Sharp, S.A. Eccles, S. Gowan, S. Popov, C. Jones, A. Pearson,
760 G. Vassal, P. Workman, Mechanistic evaluation of the novel HSP90 inhibitor
761 NVP-AUY922 in adult and pediatric glioblastoma, Mol. Cancer Ther. 9 (2010)
762 1219–1233. doi:10.1158/1535-7163.MCT-09-0683.
763 [27] B. Newman, Y. Liu, H.F. Lee, D. Sun, Y. Wang, HSP90 inhibitor 17-AAG
764 selectively eradicates lymphoma stem cells, Cancer Res. 72 (2012) 4551–4561.

765 doi:10.1158/0008-5472.CAN-11-3600.
766 [28] S.A. Eccles, A. Massey, F.I. Raynaud, S.Y. Sharp, G. Box, M. Valenti, L.
767 Patterson, A. de Haven Brandon, S. Gowan, F. Boxall, W. Aherne, M. Rowlands,
768 A. Hayes, V. Martins, F. Urban, K. Boxall, C. Prodromou, L. Pearl, K. James,
769 T.P. Matthews, K.M. Cheung, A. Kalusa, K. Jones, E. McDonald, X. Barril, P.A.
770 Brough, J.E. Cansfield, B. Dymock, M.J. Drysdale, H. Finch, R. Howes, R.E.
771 Hubbard, A. Surgenor, P. Webb, M. Wood, L. Wright, P. Workman, NVP-
772 AUY922: a novel heat shock protein 90 inhibitor active against xenograft tumor
773 growth, angiogenesis, and metastasis, Cancer Res. 68 (2008) 2850–2860.
774 doi:10.1158/0008-5472.CAN-07-5256.
775 [29] H.B. Kim, S.H. Lee, J.H. Um, W.K. Oh, D.W. Kim, C.D. Kang, S.H. Kim,
776 Sensitization of multidrug-resistant human cancer cells to Hsp90 inhibitors by
777 down-regulation of SIRT1, Oncotarget. 6 (2015) 36202–36218.
778 doi:10.18632/oncotarget.5343.
779 [30] T. Shimamura, S.A. Perera, K.P. Foley, J. Sang, S.J. Rodig, T. Inoue, L. Chen, D.
780 Li, J. Carretero, Y.C. Li, P. Sinha, C.D. Carey, C.L. Borgman, J.P. Jimenez, M.
781 Meyerson, W. Ying, J. Barsoum, K.K. Wong, G.I. Shapiro, I. Geoffrey,
782 Ganetespib (STA-9090), a nongeldanamycin HSP90 inhibitor, has potent
783 antitumor activity in in vitro and in vivo models of non-small cell lung cancer,
784 Clin Cancer Res. 18 (2012) 4973–4985. doi:10.1158/1078-0432.CCR-11-2967.
785 [31] Clinical Trials, (2020).
786 https://clinicaltrials.gov/ct2/results?cond=Cancer&term=HSP90+inhibitor&cntry
787 =&state=&city=&dist=.
788 [32] D.B. Solit, S.P. Ivy, C. Kopil, R. Sikorski, M.J. Morris, S.F. Slovin, W.K. Kelly,
789 A. Delacruz, T. Curley, G. Heller, S. Larson, L. Schwartz, M.J. Egorin, N.
790 Rosen, H.I. Scher, Cancer Therapy : Clinical Phase I T rial of 17-Allylamino-17-
791 Demethoxygeldanamycin in Patients with Advanced Cancer, 13 (2007) 1775–
792 1782. doi:10.1158/1078-0432.CCR-06-1863.
793 [33] D. Zhou, Y. Liu, J. Ye, W. Ying, L.S. Ogawa, T. Inoue, N. Tatsuta, Y. Wada, K.
794 Koya, Q. Huang, R.C. Bates, A.J. Sonderfan, A rat retinal damage model predicts
795 for potential clinical visual disturbances induced by Hsp90 inhibitors, Toxicol
796 Appl Pharmacol. 273 (2013) 401–409. doi:10.1016/j.taap.2013.09.018.

797 [34] G. Hallur, A. Sivramakrishnan, S. V Bhat, Three New Tetranortriterpenoids from
798 Neem Seed Oil, J. Nat. Prod. 65 (2002) 1177–1179. doi:10.1021/np0105174.
799 [35] G.E. Brandt, M.D. Schmidt, T.E. Prisinzano, B.S. Blagg, Gedunin, a novel hsp90
800 inhibitor: semisynthesis of derivatives and preliminary structure-activity
801 relationships, J Med Chem. 51 (2008) 6495–6502. doi:10.1021/jm8007486.
802 [36] C.A. Patwardhan, A. Fauq, L.B. Peterson, C. Miller, B.S. Blagg, A. Chadli,
803 Gedunin inactivates the co-chaperone p23 protein causing cancer cell death by
804 apoptosis, J Biol Chem. 288 (2013) 7313–7325. doi:10.1074/jbc.M112.427328.
805 [37] R.L. Matts, G.E. Brandt, Y. Lu, A. Dixit, M. Mollapour, S. Wang, A.C.
806 Donnelly, L. Neckers, G. Verkhivker, B.S. Blagg, A systematic protocol for the
807 characterization of Hsp90 modulators, Bioorg Med Chem. 19 (2011) 684–692.
808 doi:10.1016/j.bmc.2010.10.029.
809 [38] R. Subramani, E. Gonzalez, S.B. Nandy, A. Arumugam, F. Camacho, J. Medel,
810 D. Alabi, R. Lakshmanaswamy, Gedunin inhibits pancreatic cancer by altering
811 sonic hedgehog signaling pathway, Oncotarget. 8 (2017) 10891–10904.
812 doi:10.18632/oncotarget.8055.
813 [39] S.G. Kamath, N. Chen, Y. Xiong, R. Wenham, S. Apte, M. Humphrey, J.
814 Cragun, J.M. Lancaster, Gedunin, a novel natural substance, inhibits ovarian
815 cancer cell proliferation, Int J Gynecol Cancer. 19 (2009) 1564–1569.
816 doi:10.1111/IGC.0b013e3181a83135.
817 [40] S.J. Uddin, L. Nahar, J.A. Shilpi, M. Shoeb, T. Borkowski, S. Gibbons, M.
818 Middleton, M. Byres, S.D. Sarker, Gedunin, a limonoid from Xylocarpus
819 granatum, inhibits the growth of CaCo-2 colon cancer cell line in vitro, Phytother
820 Res. 21 (2007) 757–761. doi:10.1002/ptr.2159.
821 [41] K.K. Kishore T, R. Ganugula, D.R. Gade, G.B. Reddy, S. Nagini, Gedunin
822 abrogates aldose reductase, PI3K/Akt/mToR, and NF-κB signaling pathways to
823 inhibit angiogenesis in a hamster model of oral carcinogenesis, Tumour Biol. 37
824 (2015) 2083–2093. doi:10.1007/s13277-015-4003-0.
825 [42] C. Kilkenny, W.J. Browne, I.C. Cuthill, M. Emerson, D.G. Altman, Improving
826 bioscience research reporting: the ARRIVE guidelines for reporting animal
827 research, Osteoarthr. Cartil. 20 (2012) 256–260.
828 doi:10.1016/J.JOCA.2012.02.010.

829 [43] C.-C. Liang, A.Y. Park, J.-L. Guan, In vitro scratch assay: a convenient and
830 inexpensive method for analysis of cell migration in vitro, Nat. Protoc. 2 (2007)
831 329–333. doi:10.1038/nprot.2007.30.
832 [44] S. Cha, G. Johnson, Y.Z. Wadghiri, O. Jin, J. Babb, D. Zagzag, D.H. Turnbull,
833 Dynamic, Contrast-Enhanced Perfusion MRI in Mouse Gliomas : Correlation
834 With Histopathology, 855 (2003) 848–855. doi:10.1002/mrm.10446.
835 [45] G. Paxinos, K.B.J. Franklin, The mouse brain in stereotaxic coordinates: hard
836 cover edition., Acad. Press. 2nd Editio (2001) 360.
837 https://www.elsevier.com/books/paxinos-and-franklins-the-mouse-brain-in-
838 stereotaxic-coordinates-compact/franklin/978-0-12-816159-3 (acessado 14 de
839 agosto de 2021).
840 [46] CCAC GUIDELINES, Can. Vet. J. 44 (2003) 631.
841 https://www.ncbi.nlm.nih.gov/pmc/articles/PMC340226/.
842 [47] I. Vermes, C. Haanen, H. Steffens-Nakken, C. Reutellingsperger, A novel assay
843 for apoptosis Flow cytometric detection of phosphatidylserine expression on
844 early apoptotic cells using fluorescein labelled Annexin V, J. Immunol. Methods.
845 184 (1995) 39–51. doi:https://doi.org/10.1016/0022-1759(95)00072-I.
846 [48] G. Barroso, S. Taylor, M. Morshedi, F. Manzur, F. Gaviño, S. Oehninger,
847 Mitochondrial membrane potential integrity and plasma membrane translocation
848 of phosphatidylserine as early apoptotic markers: a comparison of two different
849 sperm subpopulations, Fertil. Steril. 85 (2006) 149–154.
850 doi:https://doi.org/10.1016/j.fertnstert.2005.06.046.
851 [49] J. Skommer, D. Wlodkowic, W. Telford, J. Skommer, Z. Darzynkiewicz,
852 Apoptosis and beyond: cytometry in studies of programmed cell death, Methods
853 Cell Biol. 103 (2011) 55–98. doi:10.1016/B978-0-12-385493-3.00004-8.
854 [50] A. Wells, J. Grahovac, S. Wheeler, B. Ma, D. Lauffenburger, Targeting tumor
855 cell motility as a strategy against invasion and metastasis, Trends Pharmacol. Sci.
856 34 (2013) 283–289. doi:https://doi.org/10.1016/j.tips.2013.03.001.
857 [51] R.J. Eddy, M.D. Weidmann, V.P. Sharma, J.S. Condeelis, Tumor Cell
858 Invadopodia: Invasive Protrusions that Orchestrate Metastasis, Trends Cell Biol.
859 27 (2017) 595–607. doi:https://doi.org/10.1016/j.tcb.2017.03.003.
860 [52] J. Winkler, A. Abisoye-Ogunniyan, K.J. Metcalf, Z. Werb, Concepts of

861 extracellular matrix remodelling in tumour progression and metastasis, Nat.
862 Commun. 11 (2020) 5120. doi:10.1038/s41467-020-18794-x.
863 [53] J. Folkman, Angiogenesis in cancer, vascular, rheumatoid and other disease, Nat.
864 Med. 1 (1995) 27–30. doi:10.1038/nm0195-27.
865 [54] J. Folkman, Angiogenesis: an organizing principle for drug discovery?, 6 (2007)
866 273–286.
867 [55] T.C.G.A. TCGA, Comprehensive genomic characterization defines human
868 glioblastoma genes and core pathways, Nature. 455 (2008) 1061–1068.
869 doi:10.1038/nature07385.
870 [56] J. Langhans, L. Schneele, N. Trenkler, H. von Bandemer, L. Nonnenmacher, G.
871 Karpel-Massler, M.D. Siegelin, S. Zhou, M.-E. Halatsch, K.-M. Debatin, M.-A.
872 Westhoff, The effects of PI3K-mediated signalling on glioblastoma cell
873 behaviour, Oncogenesis. 6 (2017) 398. doi:10.1038/s41389-017-0004-8.
874 [57] D. Chen, D. Zuo, C. Luan, M. Liu, M. Na, L. Ran, Y. Sun, A. Persson, E.
875 Englund, L.G. Salford, E. Renström, X. Fan, E. Zhang, Glioma cell proliferation
876 controlled by ERK activity-dependent surface expression of PDGFRA, PLoS
877 One. 9 (2014). doi:10.1371/journal.pone.0087281.
878 [58] V. Frattini, V. Trifonov, J.M. Chan, A. Castano, M. Lia, F. Abate, S.T. Keir,
879 A.X. Ji, P. Zoppoli, F. Niola, C. Danussi, I. Dolgalev, P. Porrati, S. Pellegatta, A.
880 Heguy, G. Gupta, D.J. Pisapia, P. Canoll, J.N. Bruce, R.E. McLendon, H. Yan,
881 K. Aldape, G. Finocchiaro, T. Mikkelsen, G.G. Privé, D.D. Bigner, A. Lasorella,
882 R. Rabadan, A. Iavarone, The integrated landscape of driver genomic alterations
883 in glioblastoma, Nat. Genet. 45 (2013) 1141–1149. doi:10.1038/ng.2734.
884 [59] M. Miyai, H. Tomita, A. Soeda, H. Yano, T. Iwama, A. Hara, Current trends in
885 mouse models of glioblastoma, J. Neurooncol. 135 (2017) 423–432.
886 doi:10.1007/s11060-017-2626-2.
887 [60] E.W. Newcomb, D. Zagzag, CNS Cancer, CNS Cancer. (2009) 227–241.
888 doi:10.1007/978-1-60327-553-8.
889 [61] V.A. Kudryavtsev, A. V. Khokhlova, V.A. Mosina, E.I. Selivanova, A.E.
890 Kabakov, Induction of Hsp70 in tumor cells treated with inhibitors of the Hsp90
891 activity: A predictive marker and promising target for radiosensitization, PLoS
892 One. 12 (2017) 1–26. doi:10.1371/journal.pone.0173640.

[62] R. Bagatell, G.D. Paine-Murrieta, C.W. Taylor, E.J. Pulcini, S. Akinaga, I.J. Benjamin, L. Whitesell, Induction of a heat shock factor 1-dependent stress response alters the cytotoxic activity of Hsp90-binding agents, Clin. Cancer Res. 6 (2000) 3312–3318.

[63] L.R. Kelland, S.Y. Sharp, P.M. Rogers, T.G. Myers, P. Workman, DT-Diaphorase expression and tumor cell sensitivity to 17-allylamino, 17-demethoxygeldanamycin, an inhibitor of heat shock protein 90, J Natl Cancer Inst. 91 (1999) 1940–1949. https://www.ncbi.nlm.nih.gov/pubmed/10564678.

[64] R.B. BADISA, S.F. DARLING-REED, P. JOSEPH, J.S. COOPERWOOD, L.M. LATINWO, C.B. GOODMAN, Selective Cytotoxic Activities of Two Novel Synthetic Drugs on Human Breast Carcinoma MCF-7 Cells, Anticancer Res. 29 (2009) 2993 LP – 2996. http://ar.iiarjournals.org/content/29/8/2993.abstract.

[65] W. Zhou, D.R. Wahl, Metabolic Abnormalities in Glioblastoma and Metabolic Strategies to Overcome Treatment Resistance, Cancers (Basel). 11 (2019) 1231. doi:10.3390/cancers11091231.

[66] M.G. Ormerod, F. Paul, M. Cheetham, X. -M Sun, Discrimination of apoptotic thymocytes by forward light scatter, Cytometry. 21 (1995) 300–304. doi:10.1002/cyto.990210311.

[67] S.M. Faisal, A. Comba, M.L. Varela, A.E. Argento, E. Brumley, C. Abel, M.G. Castro, P.R. Lowenstein, The complex interactions between the cellular and non-cellular components of the brain tumor microenvironmental landscape and their therapeutic implications, Front. Oncol. 12 (2022). https://www.frontiersin.org/articles/10.3389/fonc.2022.1005069.

[68] F. Seker-Polat, N. Pinarbasi Degirmenci, I. Solaroglu, T. Bagci-Onder, Tumor Cell Infiltration into the Brain in Glioblastoma: From Mechanisms to Clinical Perspectives., Cancers (Basel). 14 (2022). doi:10.3390/cancers14020443.

[69] E.W. Newcomb, Y. Lukyanov, T. Schnee, M. Esencay, I. Fischer, D. Hong, Y. Shao, D. Zagzag, The geldanamycin analogue 17-allylamino-17-demethoxygeldanamycin inhibits the growth of GL261 glioma cells in vitro and in vivo, Anticancer. Drugs. 18 (2007) 875–882. doi:10.1097/CAD.0b013e3281430df8.

[70] B.K. Eustace, T. Sakurai, J.K. Stewart, D. Yimlamai, C. Unger, C. Zehetmeier,

925 B. Lain, C. Torella, S.W. Henning, G. Beste, B.T. Scroggins, L. Neckers, L.L.
926 Ilag, D.G. Jay, Functional proteomic screens reveal an essential extracellular role
927 for hsp90 alpha in cancer cell invasiveness, Nat Cell Biol. 6 (2004) 507–514.
928 doi:10.1038/ncb1131.
929 [71] E.C. Brantley, E.N. Benveniste, Signal Transducer and Activator of
930 Transcription-3: A Molecular Hub for Signaling Pathways in Gliomas, Mol.
931 Cancer Res. 6 (2008) 675. doi:10.1158/1541-7786.MCR-07-2180.
932 [72] F. Azuaje, K. Tiemann, S.P. Niclou, Therapeutic control and resistance of the
933 EGFR-driven signaling network in glioblastoma, Cell Commun. Signal. 13
934 (2015) 23. doi:10.1186/s12964-015-0098-6.
935 [73] G.L. Johnson, R. Lapadat, Mitogen-Activated Protein Kinase Pathways Mediated
936 by ERK, JNK, and p38 Protein Kinases, Science (80-.). 298 (2002) 1911.
937 doi:10.1126/science.1072682.
938 [74] D.I. Duron, W. Lei, N.K. Barker, C. Stine, S. Mishra, B.S.J. Blagg, P.R.
939 Langlais, J.M. Streicher, Inhibition of Hsp90 in the spinal cord enhances the
940 antinociceptive effects of morphine by activating an ERK-RSK pathway., Sci.
941 Signal. 13 (2020). doi:10.1126/scisignal.aaz1854.
942 [75] J.M. Streicher, The Role of Heat Shock Proteins in Regulating Receptor Signal
943 Transduction, Mol. Pharmacol. 95 (2019) 468 LP – 474.
944 doi:10.1124/mol.118.114652.
945 [76] G. Niu, K.L. Wright, M. Huang, L. Song, E. Haura, J. Turkson, S. Zhang, T.
946 Wang, D. Sinibaldi, D. Coppola, R. Heller, L.M. Ellis, J. Karras, J. Bromberg, D.
947 Pardoll, R. Jove, Constitutive Stat3 activity up-regulates VEGF expression and
948 tumor angiogenesis, (2008) 2000–2008. doi:10.1038/sj/onc/1205260.
949 [77] Q. Xu, J. Briggs, S. Park, G. Niu, M. Kortylewski, S. Zhang, T. Gritsko, J.
950 Turkson, H. Kay, G.L. Semenza, J.Q. Cheng, R. Jove, H. Yu, Targeting Stat3
951 blocks both HIF-1 and VEGF expression induced by multiple oncogenic growth
952 signaling pathways, Oncogene. (2005). doi:10.1038/sj.onc.1208719.
953 [78] K. Palmowski, O. Winz, A. Rix, J. Bzyl, F.F. Behrendt, F.A. Verburg, F.M.
954 Mottaghy, M. Palmowski, Accuracy of a clinical PET/CT vs. a preclinical μPET
955 system for monitoring treatment effects in tumour xenografts., Eur. J. Radiol. 82
956 (2013) 1318–1324. doi:10.1016/j.ejrad.2013.01.028.

[79] S. Kirschner, B. Mürle, M. Felix, A. Arns, C. Groden, F. Wenz, A. Hug, G. Glatting, M. Kramer, F.A. Giordano, M.A. Brockmann, Imaging of Orthotopic Glioblastoma Xenografts in Mice Using a Clinical CT Scanner: Comparison with Micro-CT and Histology, PLoS One. 11 (2016) e0165994. doi:10.1371/journal.pone.0165994.

[80] M.A. Hofman, Size and Shape of the Cerebral Cortex in Mammals, Brain. Behav. Evol. 32 (1988) 17–26. doi:10.1159/000116529.

[81] M. Hofman, Evolution of the human brain: when bigger is better, Front. Neuroanat..8 (2014) 15. https://www.frontiersin.org/article/10.3389/fnana.2014.00015.

[82] A. Welch, M. Mingarelli, G. Riedel, B. Platt, Mapping changes in mouse brain metabolism with PET/CT., J. Nucl. Med. 54 (2013) 1946–1953. doi:10.2967/jnumed.113.121509.

[83] N. Ferrara, Pathways mediating VEGF-independent tumor angiogenesis, Cytokine Growth Factor Rev. 21 (2010) 21–26. doi:https://doi.org/10.1016/j.cytogfr.2009.11.003.